

This discussion paper is/has been under review for the journal Atmospheric Chemistry and Physics (ACP). Please refer to the corresponding final paper in ACP if available.

# Tropospheric aerosol scattering and absorption over Central Europe: a closure study for the dry particle state

N. Ma<sup>1,2</sup>, W. Birmili<sup>1</sup>, T. Müller<sup>1</sup>, T. Tuch<sup>1</sup>, Y. F. Cheng<sup>3</sup>, W. Y. Xu<sup>2</sup>, C. S. Zhao<sup>2</sup>, and A. Wiedensohler<sup>1</sup>

<sup>1</sup>Leibniz Institute for Tropospheric Research, Permoserstr. 15, 04318 Leipzig, Germany

<sup>2</sup>Department of Atmospheric and Oceanic Sciences, School of Physics, Peking University, 100871 Beijing, China

<sup>3</sup>Multiphase Chemistry Department, Max Planck Institute for Chemistry, 55020 Mainz, Germany

Received: 24 September 2013 – Accepted: 15 October 2013 – Published: 28 October 2013

Correspondence to: N. Ma (muran1984@gmail.com)

Published by Copernicus Publications on behalf of the European Geosciences Union.

## Tropospheric aerosol scattering and absorption over Central Europe

N. Ma et al.

Title Page

Abstract

Introduction

Conclusions

References

Tables

Figures

⏪

⏩

◀

▶

Back

Close

Full Screen / Esc

Printer-friendly Version

Interactive Discussion

## Abstract

This work analyses optical properties of the dry tropospheric aerosol measured at the regional GAW observation site Melpitz in East Germany. For a continuous observation period between 2007 and 2010, we provide representative values of the dry-state scattering coefficient, the hemispheric backscattering coefficient, the absorption coefficient, single scattering albedo, and the Ångström exponent. Besides the direct measurement, the aerosol scattering coefficient was alternatively computed from experimental particle number size distributions using a Mie code. Within pre-defined limits, a closure could be achieved with the direct measurement. The achievement of closure implies that such calculations can be used as a high-level quality control measure for data sets involving multiple instrumentation.

All dry optical properties showed significant annual variations, which were attributed to corresponding variations in the regional emission fluxes, the intensity of secondary particle formation, and the mixed layer height. Air mass classification showed that atmospheric stability is a major factor influencing the dry aerosol properties at the GAW station. In the cold season, temperature inversions limit the volume available for atmospheric mixing, so that the aerosol optical properties near the ground proved quite sensitive to the geographical origin of the air mass. In the warm season, when the atmosphere is usually well-mixed during day-time, considerably less variability was observed for the optical properties between different air masses. This work provides, on the basis of quality-checked in-situ measurements, a first step towards a climatological assessment of direct aerosol radiative forcing in the region under study.

## 1 Introduction

Atmospheric aerosols influence the earth's radiation budget in several ways: First, by directly scattering and absorbing solar radiation (Charlson et al., 1992), and second, by acting as cloud condensation nuclei and thus affecting the optical properties and

ACPD

13, 27811–27854, 2013

## Tropospheric aerosol scattering and absorption over Central Europe

N. Ma et al.

Title Page

Abstract

Introduction

Conclusions

References

Tables

Figures

⏪

⏩

◀

▶

Back

Close

Full Screen / Esc

Printer-friendly Version

Interactive Discussion



## Tropospheric aerosol scattering and absorption over Central Europe

N. Ma et al.

Title Page

Abstract

Introduction

Conclusions

References

Tables

Figures

⏪

⏩

◀

▶

Back

Close

Full Screen / Esc

Printer-friendly Version

Interactive Discussion

lifetimes of clouds (Twomey, 1974; Albrecht, 1989; Rosenfeld, 1999, 2000). The radiative forcing caused by these two effects is estimated as  $-0.5 \text{ W m}^{-2}$  and  $-0.7 \text{ W m}^{-2}$ , respectively, with their uncertainties being the largest among all climate forcing factors (IPCC, 2007). Very differently from the well-mixed greenhouse gases such as  $\text{CO}_2$  and methane, aerosols show considerable spatial and temporal inhomogeneities in the atmosphere (van Donkelaar et al., 2010; Liu et al., 2009). This makes an assessment of aerosol-related climate-effects substantially more complicated than those related to greenhouse gases.

Satellites monitor aerosol optical properties on a global scale. However, the determination of aerosol-related radiative forcing on the basis of satellites measurements requires assumptions for certain microphysical aerosol optical parameters that cannot be measured by satellites (Tanré et al., 1997). Variations in these aerosol parameters, as they naturally occur in the atmosphere, can propagate into considerable uncertainties in the satellite-retrieved aerosol properties. In-situ studies of the spatial and temporal variation of aerosol optical properties are therefore a vital step in reducing the uncertainty of radiative forcing effects derived from passive remote sensing data (Delene et al., 2002).

Also, the aerosol optical properties and their uncertainties are very important for modelers. Long-term measurement of aerosol optical properties can be used to develop the parameterizations for important properties and further used in models, reducing the uncertainties induced by the insufficiency of information on aerosol properties.

Long term in-situ observations of aerosol optical properties (i.e. longer than one year) have seldom been reported, and no such observations have been described for the Central European troposphere. To close this gap, we collected a body of dry aerosol number size distributions, aerosol scattering and absorption coefficients at the research station Melpitz in East Germany between 2007 to 2010. This paper discusses the measured values on a statistical basis, and analyses temporal variations of the parameters. Aerosol scattering and absorption coefficients are calculated from experimental particle number size distributions, striving for a closure with the directly measured values.



at wavelengths of 450, 550 and 700 nm. Checks with particle-free zero air were performed four times per day. The truncation and non-Lambertian errors were corrected for the whole dataset using the most up-to-date method (Sect. 3.2).

The aerosol absorption coefficient ( $\sigma_{\text{ap}}$ ) for dry aerosols was measured with a Multi-angle Absorption Photometer (MAAP Model 5012, Thermo, Inc., Waltham, MA USA; Petzold and Schönlinner, 2004) at a wavelength of 637 nm (Müller et al., 2011). The instrument provides mass concentrations of black carbon (BC) in  $\mu\text{g m}^{-3}$ . Following the user manual, the originally measured  $\sigma_{\text{ap}}$  was retrieved by dividing this value by the mass absorption coefficient of  $6.6 \text{ m}^2 \text{ g}^{-1}$ .

A Twin Differential Mobility Particle Sizer (TDMPS; Birmili et al., 1999) measured dry aerosol number size distributions for the mobility diameter range 3–800 nm. The measurements were performed in compliance with recently issued guidelines for atmospheric particle size distribution measurements (Wiedensohler et al., 2012). Briefly, the evaluation of particle number size distributions involved a multiple charge correction (Pfeifer et al., 2013), corrections for the counting efficiency of the condensation particle counters (Wiedensohler et al., 1997), and corrections for the transmission losses in the differential mobility analyser, and all the internal and external plumbing of the instrument. The accuracy of the TDMPS number size distributions is estimated to be  $\pm 10\%$  with respect to number concentration, and  $\pm 3\%$  with respect to particle sizing.

An Aerodynamic Particle Sizer (APS Model 3320, TSI, Inc., Shoreview, MN USA) was employed to measure dry aerosol number size distributions for aerodynamic diameters between 0.5 and 10  $\mu\text{m}$ . Electrical mobility diameters from the TDMPS and aerodynamic diameters from the APS were converted to volume equivalent diameters according to DeCarlo et al. (2004), assuming size-dependent gravimetric densities and shape factors. The particle densities for fine and coarse mode were assumed to be  $1.6 \text{ g cm}^{-3}$  and  $2.5 \text{ g cm}^{-3}$ , and the shape factors as 1.0 and 1.26, respectively. After these adjustments, the TDMPS and APS distributions were merged to a continuous distribution ranging from 3 nm to 10  $\mu\text{m}$ .

## Tropospheric aerosol scattering and absorption over Central Europe

N. Ma et al.

[Title Page](#)[Abstract](#)[Introduction](#)[Conclusions](#)[References](#)[Tables](#)[Figures](#)[⏪](#)[⏩](#)[◀](#)[▶](#)[Back](#)[Close](#)[Full Screen / Esc](#)[Printer-friendly Version](#)[Interactive Discussion](#)

## 2.2 Optical closure for dry aerosol

Closure studies are useful to estimate the uncertainties of measurement techniques on the one hand, and numerical models on the other hand (Quinn et al., 1996). Here, we performed a closure study for the dry aerosol optical properties as part of an examination of the quality of our ambient aerosol measurements. Concretely, the measured  $\sigma_{\text{sp}}$  and  $\sigma_{\text{bsp}}$  were compared with the corresponding values computed from the particle number size distribution measurements using a Mie code. The calculation was based on a modified Mie model which accounts for the truncation and non-Lambertian effect of TSI 3563 nephelometer.

For the calculation of dry  $\sigma_{\text{sp}}$  and  $\sigma_{\text{bsp}}$ , the particulate species are divided into two fundamental groups. These include, on the one hand, light-absorbing carbon and, on the other hand, the less absorbing components including sulfate, nitrate, ammonium, organic matter, and other undetermined compounds (cf. Wex et al., 2002). Although the chemical composition within this latter group is rather different, the refractive indices of these less absorbing species are basically very similar, implying similar optical properties. Representative refractive indices for these two groups were extracted from a range of literature sources (Ouimette and Flagan, 1982; Hasan and Dzubay, 1983; Sloane, 1984; Seinfeld and Pandis, 1998; Covert et al., 1990; Tang and Munkelwitz, 1994), yielding 1.75–0.55i for light-absorbing carbon and 1.53–10<sup>-6</sup>i for the less absorbing components.

Three kinds of conceptual models are usually applied to describe the mixing state of light-absorbing carbon and less absorbing components: (1) external mixture, (2) homogeneous internal mixture and (3) core-shell internal mixture. For the external mixture, different compounds are separated as different particles; while in the internal mixture, all particles consist of the same mixture of compounds (Winkler, 1973). These conceptual models have been widely used to assess aerosol optical properties and direct radiative forcing. Among the internal mixture models, the core-shell mixture model – suggesting that light-absorbing carbon cores are surrounded by shells of less absorb-

### Tropospheric aerosol scattering and absorption over Central Europe

N. Ma et al.

[Title Page](#)[Abstract](#)[Introduction](#)[Conclusions](#)[References](#)[Tables](#)[Figures](#)[⏪](#)[⏩](#)[◀](#)[▶](#)[Back](#)[Close](#)[Full Screen / Esc](#)[Printer-friendly Version](#)[Interactive Discussion](#)

ing components, has been shown to yield more realistic results than the homogeneous internal mixture model (Jacobson et al., 2001; Chandra et al., 2004; Katrinak et al., 1992, 1993; Ma et al., 2012). Because atmospheric aerosols are likely to be a partial mixture of externally and internally mixed particles, external mixture and core-shell internal mixture were considered as the limit cases of the aerosol mixing state in this study. Homogeneous internal mixture was also considered during the calculations as a reference case.

Lacking information on size-resolved volume/mass concentration of light-absorbing carbon, its volume fraction was assumed to be size independent. The volume fraction of light-absorbing carbon ( $f_{\text{LAC}}$ ) can be calculated as:

$$f_{\text{LAC}} = \frac{m_{\text{LAC,MAAP}}}{\rho_{\text{LAC}} \cdot \sum_{D_p} \left[ \frac{\pi}{6} D_p^3 \cdot n(D_p) \cdot \Delta \log D_p \right]}, \quad (1)$$

where  $m_{\text{LAC,MAAP}}$  is the mass concentration of light-absorbing carbon measured by MAAP,  $\rho_{\text{LAC}}$  is the density of light-absorbing carbon,  $n(D_p)$  is the aerosol number size distribution measured by TDMPs and APS. In the literature (Sloane et al., 1983, 1984, 1991; Sloane and Wolff, 1985; Ouimette and Flagan, 1982; Seinfeld and Pandis, 1998), the gravimetric density of light-absorbing carbon is reported to range from  $1.00 \text{ g cm}^{-3}$  to  $2.00 \text{ g cm}^{-3}$ . An average value of  $1.5 \text{ g cm}^{-3}$  was chosen, with an estimated uncertainty of 33 % to cover a range of possible values.

For the case of external mixture, the number size distributions of light-absorbing carbon particles and less absorbing component particles can be derived with  $n_{\text{LAC}}(D_p) = n(D_p) \cdot f_{\text{LAC}}$  and  $n_{\text{less-abs}}(D_p) = n(D_p) \cdot (1 - f_{\text{LAC}})$ , respectively. For the case of core-shell internal mixture, the radii of the light-absorbing carbon core of a particle with diameter  $D_p$  can be calculated as:  $D_{\text{core}} = D_p f_{\text{LAC}}^{1/3}$ . For the case of homogeneously internal mixture, the refractive index can be derived as a volume-weighted average between the refractive indices of the two groups:

$$\tilde{m} = \tilde{m}_{\text{LAC}} \cdot f_{\text{LAC}} + \tilde{m}_{\text{less-abs}} \cdot (1 - f_{\text{LAC}}). \quad (2)$$

27817

Tropospheric aerosol scattering and absorption over Central Europe

N. Ma et al.

Title Page

Abstract

Introduction

Conclusions

References

Tables

Figures

⏪

⏩

◀

▶

Back

Close

Full Screen / Esc

Printer-friendly Version

Interactive Discussion



To simulate the measurements of TSI 3563 nephelometer, a modified BHMIE code and a modified BHCOAT code (Bohren and Huffman, 1983; Cheng et al., 2009) were used for homogeneous spherical particles and core-shell mixed spherical particles, respectively. For details for the calculations, see Ma et al. (2011).

## 2.3 Air mass classification

This paper uses a recently developed air mass classification scheme for surface-level tropospheric aerosols in Germany. The classification is based on a cluster analysis of daily backtrajectories and radiosounding profiles obtained over Germany during the period 2005–2011, and yields 13 climatologically relevant air mass types occurring in Central Europe. Details of the scheme are planned for publication in a forthcoming paper.

Briefly, the cluster algorithm is a variant of a k-means cluster algorithm that combined numerical back trajectories and radiosounding profiles for a single receptor site (Engler et al., 2007; Birmili et al., 2010). The modified method expands the method in that it relies on backtrajectories started simultaneously at nine locations spread over Germany, and on radiosoundings measured at seven locations. Thus, the cluster algorithm yields air mass types that are representative for entire Germany. 3-D-backward trajectories were calculated using a PC version of HYSPLIT, a trajectory model provided by the NOAA Air Resources Laboratory (Draxler and Hess, 2004). Back trajectories were calculated from the Global Data Assimilation System (GDAS) analysis set, which provides meteorological fields every 3 h, a spatial horizontal resolution of 1°, and a vertical resolution corresponding to the standard pressure levels (1000, 925, 850 hPa, etc.). Backward trajectories starting at 12:00 UTC and reaching 96 h back in time were computed for a starting level of 500 m above the ground. In addition, we employed radio soundings recorded daily at 12:00 UTC at seven meteorological stations in Germany. Due to the gradual evolution of the mixed layer during the day, these measurements indicate whether the boundary layer is well-mixed on a particular day or not. To make

## Tropospheric aerosol scattering and absorption over Central Europe

N. Ma et al.

Title Page

Abstract

Introduction

Conclusions

References

Tables

Figures



Back

Close

Full Screen / Esc

Printer-friendly Version

Interactive Discussion





### 3.1.1 Comparison between calculated and measured parameters

The comparisons of measured and calculated  $\sigma_{\text{sp}}$  and  $\sigma_{\text{bsp}}$  are shown in Fig. 1. It can be seen that for both  $\sigma_{\text{sp}}$  and  $\sigma_{\text{bsp}}$ , the measured and calculated values are highly correlated. Also, the values calculated on the basis of different mixing state assumptions are quite close. On average, the calculated  $\sigma_{\text{sp}}$  based on the external mixture assumption are 9.5 % and 10.8 % higher than those based on the assumption of a homogeneous internal mixture and the core-shell internal mixture, respectively. The calculated  $\sigma_{\text{bsp}}$  based on the external mixture assumption are 16.6 % higher and 4.6 % lower than those based on the assumption of a homogeneous internal mixture and the core-shell internal mixture, respectively. The variations in calculated  $\sigma_{\text{bsp}}$  are larger than those for  $\sigma_{\text{sp}}$ , because  $\sigma_{\text{bsp}}$  reacts more sensitively to changes in the mixing state of light-absorbing carbon than  $\sigma_{\text{sp}}$  (Ma et al., 2012).

Linear fits were performed to quantify the correlation between measured and calculated  $\sigma_{\text{sp}}$  and  $\sigma_{\text{bsp}}$ . The relationship between measured and calculated values was assumed to be  $\sigma_{\text{calculated}} = b \cdot \sigma_{\text{measured}}$ . As can be seen in Fig. 1, the data points recorded at the Melpitz site spread over 3 orders of magnitudes. If the fitting was applied in linear coordinates, points with large values would be overrepresented. Therefore, fitting was performed with log-scaled values using the modified formula  $\log(\sigma_{\text{calculated}}) = \log(b) + \log(\sigma_{\text{measured}})$ . Table 2 summarizes the fitting parameters ( $b$ ) and the determination coefficients ( $R^2$ ) of  $\sigma_{\text{sp}}$  and  $\sigma_{\text{bsp}}$  for all three wavelengths. It can be noted that all the  $R^2$  of  $\sigma_{\text{sp}}$  are higher than 0.98 (except for  $\sigma_{\text{sp}}$  at 700 nm based on core-shell internal mixture), indicating significant correlations between measured and calculated values. The  $R^2$  of  $\sigma_{\text{bsp}}$  are slightly lower than those of  $\sigma_{\text{sp}}$ , but still higher than 0.97. Almost all the fitting parameters  $b$  are below 1, indicating some underestimation by all model variants.

## Tropospheric aerosol scattering and absorption over Central Europe

N. Ma et al.

[Title Page](#)[Abstract](#)[Introduction](#)[Conclusions](#)[References](#)[Tables](#)[Figures](#)[⏪](#)[⏩](#)[◀](#)[▶](#)[Back](#)[Close](#)[Full Screen / Esc](#)[Printer-friendly Version](#)[Interactive Discussion](#)

### 3.1.2 Uncertainty analysis approach

It is reasonable to understand that the calculated and measured  $\sigma_{sp}$  and  $\sigma_{bsp}$  do not match exactly. Finite uncertainties are attached to the experimental data, as well as the assumed model input parameters. Next, certain assumptions underlying the model calculations might not be true and are expected to bias the calculated parameters. Therefore, the uncertainties of the input data, the assumptions underlying the models, and their propagation into the output values should be evaluated. If the measured values then fall within such a defined range, the closure can be considered to be “achieved”.

To evaluate the uncertainties of the calculated  $\sigma_{sp}$  and  $\sigma_{bsp}$  introduced by the uncertainties of the input parameters of the Mie model, a Monte Carlo simulation was used in this study. The input parameters of the Mie model include in-situ measured data (particle number size distributions and light-absorbing carbon mass concentrations) and some constants assumed beforehand (the refractive indices of light-absorbing carbon and less absorbing components, and the density of light-absorbing carbon). With the same instrumentation, the uncertainties of the measured particle number size distributions and light-absorbing carbon mass concentrations ( $m_{LAC,MAAP}$ ) were set according to Ma et al. (2011), as shown in Table 3. It should be noted that organic carbon may also have light-absorbing components, such as HUmic-Like Substances (HULIS, Graber et al., 2006). However, a constant mass absorption efficiency ( $6.6 \text{ m}^2 \text{ g}^{-1}$ ) was used by MAAP, probably causing a bias in the reported BC mass concentrations. As mentioned in Sect. 2.2, the uncertainty ( $3\sigma$ ) of the density of light-absorbing carbon was set to 33 % to cover the possible range reported in literatures. The uncertainties for the refractive indices were also chosen to agree with the values reported in literatures (Ouimette and Flagan, 1982; Hasan and Dzubay, 1983; Sloane, 1984; Seinfeld and Pandis, 1998; Covert et al., 1990; Tang and Munkelwitz, 1994), as shown in Table 3. According to Heintzenberg et al. (2006), the uncertainty of measured  $\sigma_{sp}$  and  $\sigma_{bsp}$  is estimated as 10 %.

## Tropospheric aerosol scattering and absorption over Central Europe

N. Ma et al.

Title Page

Abstract

Introduction

Conclusions

References

Tables

Figures

⏪

⏩

◀

▶

Back

Close

Full Screen / Esc

Printer-friendly Version

Interactive Discussion



Mie calculations were repeated using an independently-randomly varied set of input parameters. The random values were created forming normal distributions with standard deviations chosen according to Table 3. From the 65 282 records of the whole data set, 2000 records were selected randomly for the Monte Carlo simulation. Several hundreds of runs were done for each of the 2000 records to obtain the standard deviations of the calculated  $\sigma_{\text{sp}}$  and  $\sigma_{\text{bsp}}$  at the three wavelengths of nephelometer, and under the three assumed mixing states. And the average standard deviations of the 2000 records were considered as the standard deviations of the model results. As listed in Table 4, for different wavelengths and mixing state assumptions, the average relative standard deviations for  $\sigma_{\text{sp}}$  range from 7.99 % to 8.70 %, while those for  $\sigma_{\text{bsp}}$  range from 6.85 % to 8.02 %.

### 3.1.3 Uncertainty analysis results

Comparisons between measured and calculated  $\sigma_{\text{sp}}$  and  $\sigma_{\text{bsp}}$  were carried out taking into account the uncertainties of the measurements and the calculations. For  $\sigma_{\text{sp}}$ , the calculated values with external mixture assumption plus triple standard deviation and the calculated values with core-shell internal mixture assumption minus triple standard deviation were considered as the boundaries of the possible range within which the measured values should fall. And the calculated values with core-shell internal mixture assumption plus triple standard deviation and the calculated values with external mixture assumption minus triple standard deviation were considered as the boundaries of the possible range within which the measured  $\sigma_{\text{bsp}}$  should be. The ratios of the data records that satisfy the closure criterion were calculated and listed in Table 5. For all the three wavelengths, more than 99 % data records of  $\sigma_{\text{sp}}$  satisfied the closure criterion, whereas for  $\sigma_{\text{bsp}}$ , the ratios are a little lower, but are still above 96 %.

In conclusion, considering the uncertainties, most of the measured  $\sigma_{\text{sp}}$  and  $\sigma_{\text{bsp}}$  agree with the values calculated with a modified Mie model using measured particle number size distributions and light-absorbing carbon concentrations, confirming a stable performance of the instruments and a good quality of the data set.



## Tropospheric aerosol scattering and absorption over Central Europe

N. Ma et al.

Title Page

Abstract

Introduction

Conclusions

References

Tables

Figures

⏪

⏩

◀

▶

Back

Close

Full Screen / Esc

Printer-friendly Version

Interactive Discussion

to check whether the parameters  $a$  and  $b$  given in Anderson et al. (1998) were appropriate for Melpitz, the particle number size distributions measured from 2008 to 2010 were used to calculate alternative  $C_{\text{sp}}$  and  $C_{\text{bsp}}$  via the Mie model. In the calculation, the refractive indices were estimated as mentioned in Sect. 2.2 and the mixing state of the aerosol was assumed as homogeneously internal. Figure 2 displays the calculated  $C_{\text{sp}}$  vs. nephelometer-derived  $\alpha$  at three wavelengths. The red line is the result of the linear fitting between  $C_{\text{sp}}$  and  $\alpha$ . It is interesting that for all three wavelengths, the fitting result does not match the formula for the no-cut case in Anderson's method (the black solid line in Fig. 2. It is close to the sub- $\mu\text{m}$  case in Anderson's method (black dash line in Fig. 2 but with different intercepts. A possible reason might be that the statistical properties of the particle number size distributions measured in Melpitz differ from those used by Anderson et al. when developing their method.

In this study, the parameters derived from the linear fitting of calculated  $C_{\text{sp}}$  and  $\alpha$  were used in the correction for the four-year nephelometer data. In other words, we used Anderson's method but with a new group of parameters determined by ourselves. The new parameters are listed in Table 6. The calculated  $C_{\text{bsp}}$  for the three wavelengths were also shown.

### 3.3 Overview of long-term measurements

Figure 3 shows time series of daily average dry aerosol  $\sigma_{\text{sp}}$ ,  $\sigma_{\text{bsp}}$  and  $\sigma_{\text{ap}}$  measurements for the period of 2007 to 2010. The figure also shows the calculated single scattering albedo ( $\omega$ ), hemispheric back scattering coefficient ( $b$ ) and Ångström exponent ( $\alpha$ ). Significant seasonal variations can be found for all the aerosol optical properties. Strong fluctuations, mainly related to the change of synoptic systems, also appear in all time series.

A statistics of the optical parameters based on hourly average data are given in Table 7. In Melpitz, the mean  $\sigma_{\text{sp}}$  and  $\sigma_{\text{bsp}}$  at 550 nm are  $53.37 \pm 30.01 \text{ M m}^{-1}$  and  $5.93 \pm 2.86 \text{ M m}^{-1}$ , respectively. The mean  $\sigma_{\text{ap}}$  at 637 nm is  $5.64 \pm 3.74 \text{ M m}^{-1}$ . The ratio

between the maximum and minimum monthly mean  $\sigma_{sp}$  at 550 nm was 8 and even reached up to 10 for the  $\sigma_{ap}$  at 637 nm, implying large variations for the monthly aerosol scattering and absorption levels.

Only a few published studies reported continuous measurements of aerosol scattering and absorption properties with an observation period longer than 1 yr. Some of those results were compared with the measurements in Melpitz. Delene and Ogren (2002) reported long-term measurements of aerosol optical properties in four regional monitoring stations in North America, with observation length ranging from 3 to 7 yr, all ending at the same time in 2000. At the anthropogenically influenced continental station BND, the average  $\sigma_{sp}$  at 550 nm is  $57.7 \text{ Mm}^{-1}$ , which is slightly higher than that in Melpitz. At the rural station SGP and the anthropogenically influenced marine station WSA, the  $\sigma_{sp}$  are little lower than that in Melpitz. The  $\sigma_{sp}$  measured at the BRW station located in Alaska is only one fifth of that in Melpitz. We did not compare the  $\sigma_{ap}$ , since the  $\sigma_{ap}$  reported in Delene and Ogren (2002) were at a wavelength of 550 nm. Yan et al. (2008) reported the  $\sigma_{sp}$  and  $\sigma_{ap}$  measured from 2003 to 2005 at the Global Atmosphere Watch regional station SDZ in North China. The average  $\sigma_{sp}$  (at 525 nm) measured there is about 3 times as much as that in Melpitz (adjusted to 525 nm). Vrekoussis et al. (2005) reported two measurements of aerosol scattering and absorption at Finokalia on the Crete Island in Greece (2001–2002) and Erdemli in Turkey (1999–2000). The mean  $\sigma_{sp}$  (532 nm) in Finokalia is 10 % lower than that in Melpitz, while  $\sigma_{sp}$  in Erdemli is 60 % higher than that in Melpitz. Another study (Gerasopoulos et al., 2003) reported a three-year average  $\sigma_{sp}$  of  $65 \pm 40 \text{ Mm}^{-1}$  at a rural site in Northern Greece. This value is about 20 % higher than that in Melpitz.

The single scattering albedo  $\omega$ , defined as  $\omega = \sigma_{sp} / (\sigma_{sp} + \sigma_{ap})$ , is instrumental for the estimation of aerosol direct radiative forcing. A small error in this parameter may change the sign of aerosol radiative forcing (Takemura et al., 2002). To calculate  $\omega$  in Melpitz, the measured  $\sigma_{sp}$  and  $\sigma_{ap}$  should be corrected to the same wavelength. Lacking information on the wavelength-dependency of  $\sigma_{ap}$ , we decided to correct  $\sigma_{sp}$

## Tropospheric aerosol scattering and absorption over Central Europe

N. Ma et al.

Title Page

Abstract

Introduction

Conclusions

References

Tables

Figures

⏪

⏩

◀

▶

Back

Close

Full Screen / Esc

Printer-friendly Version

Interactive Discussion

to 637 nm using the  $\alpha$  calculated from  $\sigma_{sp}$  at 550 and 700 nm. The mean  $\omega$  at 637 nm for dry aerosols in Melpitz is  $0.871 \pm 0.019$ .

The  $b$  was calculated according to  $b = \sigma_{bsp} / \sigma_{sp}$  using measured  $\sigma_{sp}$  and  $\sigma_{bsp}$ . The mean value of  $b$  at 550 nm is  $0.126 \pm 0.013$ . The  $\alpha$  could also be calculated with measured  $\sigma_{sp}$  at different wavelengths using  $\alpha = \ln(\sigma_{\lambda_1} / \sigma_{\lambda_2}) / \ln(\lambda_2 / \lambda_1)$ . The average  $\alpha$  calculated at wavelengths of 450 and 550 nm is  $1.72 \pm 0.20$ .

### 3.4 Annual cycles of aerosol optical properties

The average annual cycles of dry aerosol optical properties in Melpitz are shown in Fig. 4. The monthly average, median and various percentile values were calculated based on hourly data. Table 8 lists the average aerosol optical properties in each month.

It can be seen in Fig. 4 that annual cycles are evident for all the dry aerosol optical properties. The  $\sigma_{sp}$  and  $\sigma_{ap}$  have nearly the same variation pattern, with relatively higher values in winter and lower values in summer. The mean values of  $\sigma_{sp}$  and  $\sigma_{ap}$  are always higher than the median values, especially in winter, indicating that heavier pollution events rather occur in winter than in summer. The annual cycles of  $\sigma_{sp}$  and  $\sigma_{ap}$  are mainly determined by the annual variation of the boundary layer height, the local emissions and pollutants transport. In winter, the local emission is higher due to a larger amount of fossil fuel combustion. The wintertime shallow mixing layer favors the accumulation of aerosol pollutants, thus causes a higher level of  $\sigma_{sp}$  and  $\sigma_{ap}$ . Moreover, the  $\sigma_{sp}$  and  $\sigma_{ap}$  may be also influenced by the air masses related to middle or large scale atmospheric motion, thus represent wide possibility distributions in winter. In summer, the boundary layer is more unstable due to surface heating and causes turbulence and vertical mixing, which results in a dilution effect for pollutant. Therefore,  $\sigma_{sp}$  and  $\sigma_{ap}$  in summer is at a relatively low level and with small variations.

The  $\omega$  only shows slight annual variations, with high values in spring and summer, and low values in fall and winter. This annual pattern might be caused by the variation of regional emission and the secondary aerosol formation. In spring and summer, sec-

## Tropospheric aerosol scattering and absorption over Central Europe

N. Ma et al.

Title Page

Abstract

Introduction

Conclusions

References

Tables

Figures

◀

▶

◀

▶

Back

Close

Full Screen / Esc

Printer-friendly Version

Interactive Discussion



## Tropospheric aerosol scattering and absorption over Central Europe

N. Ma et al.

Title Page

Abstract

Introduction

Conclusions

References

Tables

Figures

⏪

⏩

◀

▶

Back

Close

Full Screen / Esc

Printer-friendly Version

Interactive Discussion



ondary aerosol productions via photochemistry processes are efficient and results in a large fraction of non-light-absorbing components such as organic matter and sulfate in particulate matters (Poulain et al., 2011), hence yielding a relatively higher level of  $\omega$ . In fall and winter, the secondary aerosol production is inhibited, thus resulting in a relatively lower level of  $\omega$ . The annual variation of the emission rate of black carbon may also contribute to the variation of  $\omega$ .

The  $\alpha$  is mainly determined by the shape of the aerosol number size distribution.  $\alpha$  smaller than 1 indicates that the size distribution is dominated by coarse mode, and  $\alpha$  larger than 2 indicates that fine mode particles dominates the size distribution (Eck et al., 1999; Westphal and Toon, 1991). Therefore, the annual pattern of  $\alpha$  can be explained by the variation of aerosol number size distributions due to secondary particle formation. In spring and summer, new particle formation events can be found on 40 % of the days in Melpitz. During such periods, nucleation mode concentrations can increase within a short time by  $> 1$  order of magnitude, occasionally exceeding  $10^5 \text{ cm}^{-3}$  (Birmili et al., 2001). Such high concentrations of small particles cause a high level of  $\alpha$ , thus results in higher average  $\alpha$  in spring and summer compared to that in fall and winter.

Evident annual cycle can be found in  $b$ , with higher values in summer than in winter. This annual pattern can be attributed to the variation of both the number size distribution and the mixing state of particles. As mentioned above, a significant nucleation mode can be usually found in daytime in warm seasons due to the secondary aerosol formation. According to Collaud Coen et al. (2007), such a decrease in aerosol mean size may increase the  $b$ . In addition, it was found that the morphology of a black carbon core surrounded by a non-light-absorbing shell would result in a much higher  $b$  than the external mixture of same amount of both components. In summer, due to the active photochemical aging processes, black carbon is closer to the morphology of core-shell than in winter, thus causes a higher level of  $b$ .

### 3.5 Aerosol optical properties in different air masses

The four-year aerosol optical property measurements were grouped according to the daily air mass type as described in Sect. 2.3. Figure 5 illustrates the mean back trajectories of the 13 air mass types. The corresponding results and discussions are presented in this section.

Figure 6 shows the average, median and various percentile values of aerosol optical properties for the 13 air mass types. Statistics are based on hourly data. It can be seen that the distributions of  $\sigma_{\text{sp}}$  and  $\sigma_{\text{ap}}$  among the different air masses follow a similar pattern. Among all air mass types, the highest average values for both  $\sigma_{\text{sp}}$  and  $\sigma_{\text{ap}}$  occurred in stagnant air masses during the cold season (CS-ST). In this air mass type, the vertical atmospheric stratification is very stable (see Table 1) so that vertical mixing is inhibited. Local anthropogenic emitted aerosol can be trapped in a shallow layer, and the stagnant air mass favors the accumulation of pollutants. These lead to the highest level of  $\sigma_{\text{sp}}$ ,  $\sigma_{\text{ap}}$  and the mass concentration of  $\text{PM}_{10}$  (see Table 1). For the air masses in cold season, the anticyclonic type 1 (CS-A1) and cyclonic type 3 (CS-Z3) also correspond to a high level of  $\sigma_{\text{sp}}$  and  $\sigma_{\text{ap}}$ , resulting from slowly moving, continentally influenced air masses and a stable vertical stratification (see Table 1). Originating from Northern Europe, the air mass anticyclonic type 3 (CS-A3) is cleaner than CS-A2 and CS-Z3, but still with much higher  $\sigma_{\text{sp}}$  and  $\sigma_{\text{ap}}$  than the fast-moving air masses (CS-A1, CS-Z1 and CS-Z2) originating from the North Atlantic. With a minimum residence time in the continental atmosphere, the maritime air mass anticyclonic type 1 (CS-A1), cyclonic type 1 (CS-Z1) and 2 (CS-Z2) reveal low levels of  $\sigma_{\text{sp}}$  and  $\sigma_{\text{ap}}$ . Air mass CS-Z1 is the only type with unstable vertical stratification during the cold season, resulting in the lowest level of  $\sigma_{\text{sp}}$  and  $\sigma_{\text{ap}}$  among the 7 types. In the warm season, all the 6 air mass types are accompanied with unstable vertical stratification (see Table 1). Therefore, due to vertical mixing, the  $\sigma_{\text{sp}}$  and  $\sigma_{\text{ap}}$  remain at relatively low levels even for the stagnant air mass type (WS-ST), and are much lower than those for most of the types in the cold season. The air mass anticyclonic type 1 (WS-A1), anticyclonic

## Tropospheric aerosol scattering and absorption over Central Europe

N. Ma et al.

Title Page

Abstract

Introduction

Conclusions

References

Tables

Figures



Back

Close

Full Screen / Esc

Printer-friendly Version

Interactive Discussion

## Tropospheric aerosol scattering and absorption over Central Europe

N. Ma et al.

Title Page

Abstract

Introduction

Conclusions

References

Tables

Figures

⏪

⏩

◀

▶

Back

Close

Full Screen / Esc

Printer-friendly Version

Interactive Discussion

type 2 (WS-A2) and cyclonic type 3 (WS-Z3) move at a relatively lower speed, thus having long residence times in the continental atmosphere, resulting in similar levels of  $\sigma_{sp}$  and  $\sigma_{ap}$ . The air mass cyclonic type 1 (WS-Z1) is representative of unstable air with high moving speed, originating from the North Atlantic during the warm season.

The  $\sigma_{sp}$  and  $\sigma_{ap}$  accompanied with this type of air mass show the lowest levels among all the 13 types. It should be noted that the differences of  $\sigma_{sp}$  ( $\sigma_{ap}$ ) among different air mass types in the cold season are much higher than that in the warm season. This is mainly caused by the different vertical stratification stability in those two seasons. In the cold season, the stable vertical stratification provides a favorable condition for pollutant accumulation. Therefore, the levels of  $\sigma_{sp}$  and  $\sigma_{ap}$  are very sensitive to the residence time of the air mass in the continental atmosphere. During the warm season, however, strong vertical mixing in unstable air weakens such an effect and leads to similar levels of  $\sigma_{sp}$  and  $\sigma_{ap}$  for different air mass types. These results are consistent with the air mass analysis of particle number size distributions by Engler et al. (2007).

For  $\omega$ , no significant differences could be found between most of the air mass types. However, the  $\omega$  in the air masses CS-Z1 and CS-Z2 are evidently lower and show larger variability compared with those in the other air mass types. One possible reason is that these two types of air masses originate from the North Atlantic and are associated with the highest wind speeds. Such clean maritime air has only a short residence time of a few hours over the continent before reaching Melpitz. It can thus be assumed that the light-absorbing carbonaceous aerosol originates from fresh emission and thus occurs mainly as an externally mixed fraction showing a low  $\omega$ .

As a qualitative indicator of aerosol particle size (Angstrom, 1929), the Ångström exponent  $\alpha$  varied among different air mass types because of the variation of aerosol number size distributions (Fig. 6). The  $\alpha$  for the air masses in the cold season are lower than those in the warm season, and have a larger variability. Schuster et al. (2006) found that  $\alpha$  is sensitive to the effective radius of fine mode ( $D_p < 1 \mu\text{m}$ ) particles and the volume fraction of fine mode to total aerosol. For a certain range of fine mode effective radius and volume fraction, a higher  $\alpha$  can be yielded by increasing the fine





## Tropospheric aerosol scattering and absorption over Central Europe

N. Ma et al.

Title Page

Abstract

Introduction

Conclusions

References

Tables

Figures

⏪

⏩

◀

▶

Back

Close

Full Screen / Esc

Printer-friendly Version

Interactive Discussion



For the period from 2007 to 2010, the overall average of  $\sigma_{\text{sp}}$  and  $\sigma_{\text{bsp}}$  at 550 nm were  $53.37 \pm 30.01 \text{ Mm}^{-1}$  and  $5.93 \pm 2.86 \text{ Mm}^{-1}$ , respectively. The average  $\sigma_{\text{ap}}$  at 637 nm was  $5.64 \pm 3.74 \text{ Mm}^{-1}$ . Compared to other long-period measurements around the world, these values are similar as those measured in anthropogenically influenced stations in US and southern Europe, and are much lower than those measured at a regional station in North China. The average  $\omega$  at 637 nm,  $b$  at 550 nm,  $\alpha$  for 450–550 nm and  $\alpha$  for 550–700 nm are respectively  $0.872 \pm 0.019$ ,  $0.126 \pm 0.013$ ,  $1.72 \pm 0.20$  and  $1.85 \pm 0.017$ .

All observed aerosol optical parameters showed annual variations. The  $\sigma_{\text{sp}}$  and  $\sigma_{\text{ap}}$  show much higher values and variations in winter than in summer, mainly due to the annual variation of boundary layer height and the local emissions. The single scattering albedo  $\omega$  only showed a slight annual variation, which might be caused by the variation of regional emissions and the secondary aerosol formation. Both the  $b$  and the  $\alpha$  show high values in summer and low values in winter. This pattern mainly relates to the variation of aerosol number size distributions. The variation of aerosol mixing state may also contribute to the variation of  $b$ .

A recently developed air mass classification based on a cluster analysis of daily backtrajectories and radiosounding profiles was used to classify the four-year observations according to daily changes in air mass type. It was found that the atmospheric stability plays an instrumental role for the dry aerosol optical properties measured near the ground. In the cold season, the vertical stratification is overwhelmingly stable, providing a favorable condition for pollutants accumulation. The aerosol optical properties turned out to depend sensitively on the air mass' residence time over land, the region of origin. In the warm season, in contrast, the atmosphere tends to be well mixed, at least during daytime. This causes the aerosol optical properties to be less sensitive to the origin of the air mass.

*Acknowledgements.* Continuous aerosol measurements at Melpitz were supported by the German Federal Environment Ministry (BMU) grants F&E 370343200 (German title: "Erfassung der Zahl feiner und ultrafeiner Partikel in der Außenluft") and F&E 371143232 (German title: "Tren-

analysen gesundheitsgefährdender Fein- und Ultrafeinstaubfraktionen unter Nutzung der im German Ultrafine Aerosol Network (GUAN) ermittelten Immissionsdaten durch Fortführung und Interpretation der Messreihen"). We also thank Joachim Grüner for his continuous technical support at the Melpitz station.

## 5 References

Anderson, T. L., Covert, D. S., Marshall, S. F., Laucks, M. L., Charlson, R. J., Waggoner, A. P., Ogren, J. A., Caldow, R., Holm, R. L., Quant, G., Sem, J., Wiedensohler, A., Ahlquist, N. A., and Bates, T. S.: Performance characteristics of a high-sensitivity, three-wavelength total scatter/backscatter nephelometer, *J. Atmos. Ocean. Tech.*, 13, 967–986, 1996.

10 Anderson, T. L. and Ogren, J. A.: Determining aerosol radiative properties using the TSI 3563 Integrating Nephelometer, *Aerosol Sci. Tech.*, 29, 57–69, 1998.

Ångström, A.: On the atmospheric transmission of Sun radiation and on dust in the air, *Geogr. Ann.*, 11, 156–166, 1929.

Albrecht, B. A.: Aerosols, cloud microphysics, and fractional cloudiness, *Science*, 245, 1227–1230, 1989.

15 Asmi, A., Wiedensohler, A., Laj, P., Fjaeraa, A.-M., Sellegri, K., Birmili, W., Weingartner, E., Baltensperger, U., Zdimal, V., Zikova, N., Putaud, J.-P., Marinoni, A., Tunved, P., Hansson, H.-C., Fiebig, M., Kivekäs, N., Lihavainen, H., Asmi, E., Ulevicius, V., Aalto, P. P., Swietlicki, E., Kristensson, A., Mihalopoulos, N., Kalivitis, N., Kalapov, I., Kiss, G., de Leeuw, G., Henzing, B., Harrison, R. M., Beddows, D., O'Dowd, C., Jennings, S. G., Flentje, H., Weinhold, K., Meinhardt, F., Ries, L., and Kulmala, M.: Number size distributions and seasonality of submicron particles in Europe 2008–2009, *Atmos. Chem. Phys.*, 11, 5505–5538, doi:10.5194/acp-11-5505-2011, 2011.

Birmili, W., Stratmann, F., Wiedensohler, A.: Design of a DMA-based size spectrometer for a large particle size range and stable operation, *J. Aerosol Sci.*, 30, 549–533, 1999.

25 Birmili, W., Wiedensohler, A., Heintzenberg, J., and Lehmann, K.: Atmospheric particle number size distribution in central Europe, *J. Geophys. Res.*, 106, 32005–32018, 2001.

Birmili, W., Weinhold, K., Nordmann, S., Wiedensohler, A., Spindler, G., Müller, K., Herrmann, H., T. Gnauk, M. Pitz, J. Cyrus, H. Flentje, C. Nickel, T. Kuhlbusch, A. J., Löschau, G., Haase, D., Meinhardt, F., Schwerin, A., Ries, L., and Wirtz, K.: Atmospheric aerosol measurements

## Tropospheric aerosol scattering and absorption over Central Europe

N. Ma et al.

Title Page

Abstract

Introduction

Conclusions

References

Tables

Figures

⏪

⏩

◀

▶

Back

Close

Full Screen / Esc

Printer-friendly Version

Interactive Discussion



## Tropospheric aerosol scattering and absorption over Central Europe

N. Ma et al.

Title Page

Abstract

Introduction

Conclusions

References

Tables

Figures

⏪

⏩

◀

▶

Back

Close

Full Screen / Esc

Printer-friendly Version

Interactive Discussion

in the German Ultrafine Aerosol Network (GUAN): Part 1 – soot and particle number size distributions, *Gefahrst. Reinhalt. L.*, 9, 137–145, 2009.

Birmili, W., Heinke, K., Pitz, M., Matschullat, J., Wiedensohler, A., Cyrys, J., Wichmann, H.-E., and Peters, A.: Particle number size distributions in urban air before and after volatilisation, *Atmos. Chem. Phys.*, 10, 4643–4660, doi:10.5194/acp-10-4643-2010, 2010.

Bohren, C. F. and Huffman, D. R.: *Absorption and Scattering of Light by Small Particles*, John Wiley, Hoboken, NJ, USA, 1983.

Chandra, S., Satheesh, S. K., and Srinivasan, J.: Can the state of mixing of black carbon aerosols explain the mystery of “excess” atmospheric absorption?, *Geophys. Res. Lett.*, 31, L19109, doi:10.1029/2004GL020662, 2004.

Charlson, R. J., Schwartz, S. E., Hales, J. M., Cess, R. D., Coakley Jr., J. A., Hansen, J. E., and Hofmann, D. J.: Climate forcing by anthropogenic aerosols, *Science*, 255, 423–430, 1992.

Cheng, Y. F., Berghof, M., Garland, R. M., Wiedensohler, A., Wehner, B., Müller, T., Su, H., Zhang, Y. H., Achtert, P., Nowak, A., Pöschl, U., Zhu, T., Hu, M., and Zeng, L. M.: Influence of soot mixing state on aerosol light absorption and single scattering albedo during air mass aging at a polluted regional site in northeastern China, *J. Geophys. Res.*, 114, D00G10, doi:10.1029/2008JD010883, 2009.

Collaud Coen, M., Weingartner, E., Nyeki, S., Cozic, J., Henning, S., Verheggen, B., Gehrig, R., and Baltensperger, U.: Long-term trend analysis of aerosol variables at the high-alpine site Jungfraujoch, *J. Geophys. Res.*, 112, D13213, doi:10.1029/2006JD007995, 2007.

Covert, D. S., Heintzenberg, J., Hansson, H. C.: Electro-optical detection of external mixtures in aerosols, *Aerosol Sci. Tech.*, 12, 446–456, 1990.

DeCarlo, P. F., Slowik, J. G., Worsnop, D. R., Davidovits, P., and Jimenez, J. L.: Particle morphology and density characterization by combined mobility and aerodynamic diameter measurements. Part 1: Theory, *Aerosol Sci. Tech.*, 38, 1185–1205, 2004.

Delene, D. J. and Ogren, J. A.: Variability of aerosol optical properties at four North American surface monitoring sites, *J. Atmos. Sci.*, 59, 1135–1150, 2002.

Draxler, R. R. and Hess, G. D.: Description of the Hysplit\_4 Modeling System, Technical Memorandum ERL ARL-224, NOAA, Silver Spring, Maryland, 25 pp., 2004.

Eck, T., Holben, B. N., Reid, J., Dubovik, O., Smirnov, A., O’Neill, N., Slutsker, I., and Kinne, S.: Wavelength dependence of the optical depth of biomass burning, urban, and desert dust aerosols, *J. Geophys. Res.*, 104, 31333–31349, 1999.

**Tropospheric aerosol scattering and absorption over Central Europe**

N. Ma et al.

Title Page

Abstract

Introduction

Conclusions

References

Tables

Figures

◀

▶

◀

▶

Back

Close

Full Screen / Esc

Printer-friendly Version

Interactive Discussion



- Engler, C., Rose, D., Wehner, B., Wiedensohler, A., Brüggemann, E., Gnauk, T., Spindler, G., Tuch, T., and Birmili, W.: Size distributions of non-volatile particle residuals ( $D_p < 800$  nm) at a rural site in Germany and relation to air mass origin, *Atmos. Chem. Phys.*, **7**, 5785–5802, doi:10.5194/acp-7-5785-2007, 2007.
- 5 Gerasopoulos, E., Andreae, M. O., Zerefos, C. S., Andreae, T. W., Balis, D., Formenti, P., Merlet, P., Amiridis, V., and Papastefanou, C.: Climatological aspects of aerosol optical properties in Northern Greece, *Atmos. Chem. Phys.*, **3**, 2025–2041, doi:10.5194/acp-3-2025-2003, 2003.
- Graber, E. R. and Rudich, Y.: Atmospheric HULIS: How humic-like are they? A comprehensive and critical review, *Atmos. Chem. Phys.*, **6**, 729–753, doi:10.5194/acp-6-729-2006, 2006.
- 10 Hasan, H. and Dzubay, T. G.: Apportioning light extinction coefficients to chemical species in atmospheric aerosol, *Atmos. Environ.*, **17**, 1573–1581, 1983.
- Heintzenberg, J. and Charlson, R. J.: Design and applications of the integrating nephelometer: a review, *J. Atmos. Ocean. Tech.*, **13**, 987–1000, 1996.
- 15 Heintzenberg, J., Wiedensohler, A., Tuch, T. M., Covert, D. S., Sheridan, P., Ogren, J. A., Gras, J., Nessler, R., Kleefeld, C., Kalivitis, N., Aaltonen, V., Wilhei, R. T., and Havlicek, M.: Inter-comparisons and aerosol calibrations of 12 commercial integrating nephelometers of three manufacturers, *J. Atmos. Ocean. Tech.*, **23**, 902–914, 2006.
- IPCC, Climate Change 2007: The Physical Science Basis, Contribution of Working Group I to the Fourth Assessment Report of the Intergovernmental Panel on Climate Change, edited by: Solomon, S., Qin, D., Manning, M., Chen, Z., Marquis, M., Averyt, K., Tignor, M., and Miller, H. L., 996 pp., Cambridge University Press, Cambridge and New York, 2007.
- 20 Jacobson, M. Z.: Strong radiative heating due to the mixing state of black carbon in atmospheric aerosols, *Nature*, **409**, 695–697, 2001.
- 25 Katrinak, K. A., Rez, P., and Buseck, P. R.: Structural variations in individual carbonaceous particles from an urban aerosol, *Environ. Sci. Technol.*, **26**, 1967–1976, 1992.
- Katrinak, K. A., Rez, P., Perkes, P. R., and Buseck, P. R.: Fractal geometry of carbonaceous aggregates from an urban aerosol, *Environ. Sci. Technol.*, **27**, 539–547, 1993.
- Liu, P., Zhao, C., Zhang, Q., Deng, Z., Huang, M., Ma, X., and Tie, X.: Aircraft study of aerosol vertical distributions over Beijing and their optical properties, *Tellus B*, **61**, 756–767, 2009.
- 30 Ma, N., Zhao, C. S., Nowak, A., Müller, T., Pfeifer, S., Cheng, Y. F., Deng, Z.Z., Liu, P. F., Xu, W. Y., Ran, L., Yan, P., Göbel, T., Hallbauer, E., Mildenerger, K., Henning, S., Yu, J., Chen, L. L., Zhou, X. J., Stratmann, F., and Wiedensohler, A.: Aerosol optical properties in





## Tropospheric aerosol scattering and absorption over Central Europe

N. Ma et al.

Title Page

Abstract

Introduction

Conclusions

References

Tables

Figures

◀

▶

◀

▶

Back

Close

Full Screen / Esc

Printer-friendly Version

Interactive Discussion

- Tuch, T. M., Haudek, A., Müller, T., Nowak, A., Wex, H., and Wiedensohler, A.: Design and performance of an automatic regenerating adsorption aerosol dryer for continuous operation at monitoring sites, *Atmos. Meas. Tech.*, 2, 417–422, doi:10.5194/amt-2-417-2009, 2009.
- Twomey, S.: Pollution and the planetary albedo, *Atmos. Environ.*, 8, 1251–1256, 1974.
- van Donkelaar, A., Martin, R. V., Brauer, M., Kahn, R., Levy, R., Verduzco, C., and Villeneuve, P. J.: Global estimates of ambient fine particulate matter concentrations from satellite-based aerosol optical depth: development and application, *Environ. Health Persp.*, 118, 847–855, 2010.
- Vrekoussis, M., Liakakou, E., Kocak, M., Kubilay, N., Oikonomou, K., Sciare, J., and Mihalopoulos, N.: Seasonal variability of optical properties of aerosols in the Eastern Mediterranean, *Atmos. Environ.*, 39, 7083–7094, 2005.
- Westphal, D. and Toon, O.: Simulations of microphysical, radiative, and dynamical processes in a continental-scale forest fire smoke plume, *J. Geophys. Res.*, 96, 22379–22400, 1991.
- Wex, H., Neusüß, C., Wendisch, M., Stratmann, F., Koziar, C., Keil, A., Wiedensohler, A., and Ebert, M.: Particle scattering, backscattering, and absorption coefficients: an in situ closure and sensitivity study, *J. Geophys. Res.*, 107, 8122, doi:10.1029/2000JD000234, 2002.
- Wiedensohler, A., Orsini, D., Covert, D. S., Coffmann, D., Cantrell, W., Havlicek, M., Brechtel, F. J., Russell, L. M., Weber, R. J., Gras, J., Hudson, J. G., and Litchy, M.: Intercomparison study of the size-dependent counting efficiency of 26 condensation particle counters, *Aerosol Sci. Tech.*, 27, 224–242, 1997.
- Wiedensohler, A., Birmili, W., Nowak, A., Sonntag, A., Weinhold, K., Merkel, M., Wehner, B., Tuch, T., Pfeifer, S., Fiebig, M., Fjåraa, A. M., Asmi, E., Sellegri, K., Depuy, R., Venzac, H., Villani, P., Laj, P., Aalto, P., Ogren, J. A., Swietlicki, E., Williams, P., Roldin, P., Quincey, P., Hüglin, C., Fierz-Schmidhauser, R., Gysel, M., Weingartner, E., Riccobono, F., Santos, S., Grüning, C., Faloon, K., Beddows, D., Harrison, R., Monahan, C., Jennings, S. G., O’Dowd, C. D., Marinoni, A., Horn, H.-G., Keck, L., Jiang, J., Scheckman, J., McMurry, P. H., Deng, Z., Zhao, C. S., Moerman, M., Henzing, B., de Leeuw, G., Löschau, G., and Bastian, S.: Mobility particle size spectrometers: harmonization of technical standards and data structure to facilitate high quality long-term observations of atmospheric particle number size distributions, *Atmos. Meas. Tech.*, 5, 657–685, doi:10.5194/amt-5-657-2012, 2012.
- Winkler, P.: The growth of atmospheric aerosol particles as a function of the relative humidity—II An improved concept of mixed nuclei, *J. Aerosol Sci.*, 4, 373–387, 1973.

Yan, P., Tang, J., Huang, J., Mao, J. T., Zhou, X.J., Liu, Q., Wang, Z. F., and Zhou, H. G.: The measurement of aerosol optical properties at a rural site in Northern China, *Atmos. Chem. Phys.*, 8, 2229–2242, doi:10.5194/acp-8-2229-2008, 2008.

ACPD

13, 27811–27854, 2013

**Tropospheric aerosol scattering and absorption over Central Europe**

N. Ma et al.

Title Page

Abstract

Introduction

Conclusions

References

Tables

Figures



Back

Close

Full Screen / Esc

Printer-friendly Version

Interactive Discussion



## Tropospheric aerosol scattering and absorption over Central Europe

N. Ma et al.

Title Page

Abstract

Introduction

Conclusions

References

Tables

Figures

⏪

⏩

◀

▶

Back

Close

Full Screen / Esc

Printer-friendly Version

Interactive Discussion



**Table 1.** Characteristics of the 13 air mass types determined for Central Europe based on the cluster analysis of back trajectories and pseudo-potential temperature profiles across Germany.

Air mass type	Predominant period of the year	Atmospheric flow	Source region	Predominant wind direction at Melpitz	Vertical stratification at 12:00 UTC	Climatological frequency 2005–2011	Mean PM <sub>10</sub> at 53 rural background sites in Germany
CS-ST	cold season	stagnant	Central Europe	–	very stable	2.7 %	34 µg m <sup>-3</sup>
CS-A1	cold season	anticyclonic	North Atlantic	west	stable	5.8 %	16 µg m <sup>-3</sup>
CS-A2	cold season	anticyclonic	Eastern Europe	east	stable	4.1 %	32 µg m <sup>-3</sup>
CS-A3	cold season	anticyclonic	Northern Europe	north	stable	6.1 %	18 µg m <sup>-3</sup>
CS-Z1	cold season	cyclonic	North Atlantic	west	close to neutral	4.6 %	12 µg m <sup>-3</sup>
CS-Z2	cold season	cyclonic	North Atlantic	west/south-west	stable	5.6 %	12 µg m <sup>-3</sup>
CS-Z3	cold season	cyclonic	South west Europe	south-west	stable	5.7 %	23 µg m <sup>-3</sup>
WS-ST	warm season	stagnant	Central Europe	–	close to neutral	10.7 %	22 µg m <sup>-3</sup>
WS-A1	warm season	anticyclonic	North Atlantic	north-west	close to neutral	11.6 %	17 µg m <sup>-3</sup>
WS-A2	warm season	anticyclonic	Eastern Europe	north-east/east	close to neutral	9.6 %	20 µg m <sup>-3</sup>
WS-Z1	warm season	cyclonic	North Atlantic	north-west	close to neutral	11.2 %	12 µg m <sup>-3</sup>
WS-Z2	warm season	cyclonic	North Atlantic	west	close to neutral	12.5 %	13 µg m <sup>-3</sup>
WS-Z3	warm season	cyclonic	South west Europe	south-west	close to neutral	10.0 %	16 µg m <sup>-3</sup>

## Tropospheric aerosol scattering and absorption over Central Europe

N. Ma et al.

**Table 2.** The fitting parameters ( $b$  and  $R^2$ ) of the linear fittings for calculated and measured  $\sigma_{\text{sp}}$  and  $\sigma_{\text{bsp}}$ .

	$\lambda$ (nm)	Internal		Core-shell		External	
		$b$	$R^2$	$b$	$R^2$	$b$	$R^2$
$\sigma_{\text{sp}}$	450	0.8809	0.9827	0.8689	0.9815	0.9732	0.9854
	550	0.9196	0.9831	0.9093	0.9820	1.0061	0.9854
	700	0.9344	0.9801	0.9298	0.9795	1.0140	0.9825
$\sigma_{\text{bsp}}$	450	0.7419	0.9706	0.9458	0.9799	0.8883	0.9817
	550	0.7911	0.9731	0.9655	0.9811	0.9210	0.9819
	700	0.7518	0.9745	0.8727	0.9838	0.8432	0.9824

Title Page

Abstract

Introduction

Conclusions

References

Tables

Figures

⏪

⏩

◀

▶

Back

Close

Full Screen / Esc

Printer-friendly Version

Interactive Discussion

## Tropospheric aerosol scattering and absorption over Central Europe

N. Ma et al.

**Table 3.** Uncertainties of the input parameters for the retrieving algorithm, given as one standard deviation.

Parameter	Standard deviation ( $\sigma$ , %)
$D_{p,\text{TDMPs}}$	1.1
$D_{p,\text{APS}}$	3
$N_{\text{TDMPs}, 3-20 \text{ nm}}$	10
$N_{\text{TDMPs}, 20-200 \text{ nm}}$	3.3
$N_{\text{TDMPs}, 200-700 \text{ nm}}$	8.3
$N_{\text{APS}}$	3.3
$m_{\text{LAC,MAAP}}$	4
$\rho_{\text{LAC}} = 1.5 \text{ g cm}^{-3}$	11
$n_{\text{non}} = 1.53$	0.5
$i_{\text{non}} = 10^{-6}$	0
$n_{\text{LAC}} = 1.75$	4
$i_{\text{LAC}} = 0.55$	6.6

Title Page

Abstract

Introduction

Conclusions

References

Tables

Figures

◀

▶

◀

▶

Back

Close

Full Screen / Esc

Printer-friendly Version

Interactive Discussion

## Tropospheric aerosol scattering and absorption over Central Europe

N. Ma et al.

Title Page

Abstract

Introduction

Conclusions

References

Tables

Figures

⏪

⏩

◀

▶

Back

Close

Full Screen / Esc

Printer-friendly Version

Interactive Discussion

**Table 4.** Average relative standard deviations of the calculated  $\sigma_{sp}$  and  $\sigma_{bsp}$  yielded from the Monte Carlo simulation. EXT, CS-INT and H-INT denote the mixing state of external, core-shell internal and homogeneously internal, respectively.

$\lambda$ (nm)	Standard deviation of $\sigma_{sp}$ (%)			Standard deviation of $\sigma_{bsp}$ (%)		
	EXT	CS-INT	H-INT	EXT	CS-INT	H-INT
450	8.01	8.66	8.68	6.85	7.18	7.87
550	8.07	8.69	8.70	6.96	7.26	7.82
700	7.99	8.55	8.55	7.26	7.52	8.02

**Tropospheric aerosol scattering and absorption over Central Europe**

N. Ma et al.

[Title Page](#)[Abstract](#)[Introduction](#)[Conclusions](#)[References](#)[Tables](#)[Figures](#)[Back](#)[Close](#)[Full Screen / Esc](#)[Printer-friendly Version](#)[Interactive Discussion](#)

**Table 5.** The ratios of the measured  $\sigma_{\text{sp}}$  and  $\sigma_{\text{bsp}}$  satisfying the closure criterion to the total amount of the measured data, considering the uncertainties of the measurements and calculations.

$\lambda$ (nm)	$\sigma_{\text{sp}}$	$\sigma_{\text{bsp}}$
450	99.26 %	97.80 %
550	99.33 %	98.67 %
700	99.14 %	96.15 %

**Tropospheric aerosol scattering and absorption over Central Europe**

N. Ma et al.

**Table 6.** Parameters for the linear function of  $C_{\text{sp}}$ , and the average  $C_{\text{bsp}}$  used in current study.

$\lambda$ (nm)	$a_1$	$a_2$	$C_{\text{bsp}}$
450	1.185	−0.0446	0.978
550	1.180	−0.0456	0.979
700	1.165	−0.0417	0.984

Title Page

Abstract

Introduction

Conclusions

References

Tables

Figures

◀

▶

◀

▶

Back

Close

Full Screen / Esc

Printer-friendly Version

Interactive Discussion

## Tropospheric aerosol scattering and absorption over Central Europe

N. Ma et al.

Title Page

Abstract

Introduction

Conclusions

References

Tables

Figures

⏪

⏩

◀

▶

Back

Close

Full Screen / Esc

Printer-friendly Version

Interactive Discussion

**Table 7.** Statistic values of aerosol optical properties measured at dry condition for the period from 2007 to 2010 (based on hourly average data).

Parameter	$\lambda$ (nm)	Mean	S.D.	Median	Max.	Min.	Numbers
$\sigma_{\text{sp}}$ ( $\text{M m}^{-1}$ )	450	73.11	73.30	50.83	832.40	1.10	31 581
	550	53.61	58.64	34.70	666.74	0.76	31 581
	700	35.17	41.77	21.25	455.72	0.46	31 581
$\sigma_{\text{sp}}$ ( $\text{M m}^{-1}$ )	450	7.45	6.85	5.59	78.78	0.12	31 581
	550	5.97	5.69	4.39	67.47	0.07	31 581
	700	5.12	5.19	3.63	60.57	0.04	31 581
$\sigma_{\text{sp}}$ ( $\text{M m}^{-1}$ )	637	5.67	6.95	3.52	85.81	0.12	33 624
	$\omega$	637	0.871	0.051	0.877	0.994	30 842
$b$	550	0.125	0.022	0.124	0.258	0.075	31 581
$\alpha$	450–550	1.72	0.38	1.77	3.02	0.03	31 581
	550–700	1.85	0.41	1.91	4.72	0.10	31 581

## Tropospheric aerosol scattering and absorption over Central Europe

N. Ma et al.

**Table 8.** The averages and standard deviations of aerosol optical properties measured at dry condition for each month (based on hourly average data).

Parameter $\lambda$ (nm)	$\sigma_{\text{sp}}$ ( $\text{Mm}^{-1}$ )		$\omega$ 637	$b$ 550	$\alpha$	
	550	637			450–550	550–700
Jan	111.83 ± 112.87	11.43 ± 14.26	0.857 ± 0.048	0.111 ± 0.016	1.44 ± 0.36	1.67 ± 0.38
Feb	86.61 ± 82.50	8.45 ± 8.50	0.872 ± 0.051	0.110 ± 0.017	1.59 ± 0.34	1.83 ± 0.37
Mar	47.33 ± 41.82	4.23 ± 3.76	0.892 ± 0.049	0.118 ± 0.017	1.64 ± 0.38	1.87 ± 0.47
Apr	61.96 ± 52.69	5.36 ± 3.79	0.888 ± 0.044	0.121 ± 0.019	1.75 ± 0.28	1.99 ± 0.35
May	34.98 ± 21.78	2.90 ± 1.73	0.889 ± 0.043	0.133 ± 0.020	1.90 ± 0.26	2.02 ± 0.34
Jun	31.91 ± 24.70	2.57 ± 1.51	0.891 ± 0.039	0.140 ± 0.021	1.93 ± 0.33	1.98 ± 0.41
Jul	28.99 ± 19.06	2.79 ± 1.71	0.878 ± 0.041	0.143 ± 0.018	1.99 ± 0.28	1.98 ± 0.37
Aug	30.15 ± 23.13	3.03 ± 1.70	0.867 ± 0.048	0.140 ± 0.022	1.92 ± 0.30	1.96 ± 0.36
Sep	33.30 ± 29.01	4.04 ± 2.93	0.850 ± 0.056	0.134 ± 0.020	1.79 ± 0.32	1.81 ± 0.42
Oct	57.25 ± 45.69	6.62 ± 4.72	0.859 ± 0.049	0.118 ± 0.019	1.63 ± 0.31	1.75 ± 0.33
Nov	55.93 ± 53.70	6.84 ± 6.41	0.853 ± 0.056	0.117 ± 0.019	1.50 ± 0.39	1.64 ± 0.44
Dec	80.34 ± 70.35	9.76 ± 9.43	0.862 ± 0.054	0.111 ± 0.017	1.46 ± 0.40	1.67 ± 0.39

## Tropospheric aerosol scattering and absorption over Central Europe

N. Ma et al.

Title Page

Abstract

Introduction

Conclusions

References

Tables

Figures

◀

▶

◀

▶

Back

Close

Full Screen / Esc

Printer-friendly Version

Interactive Discussion

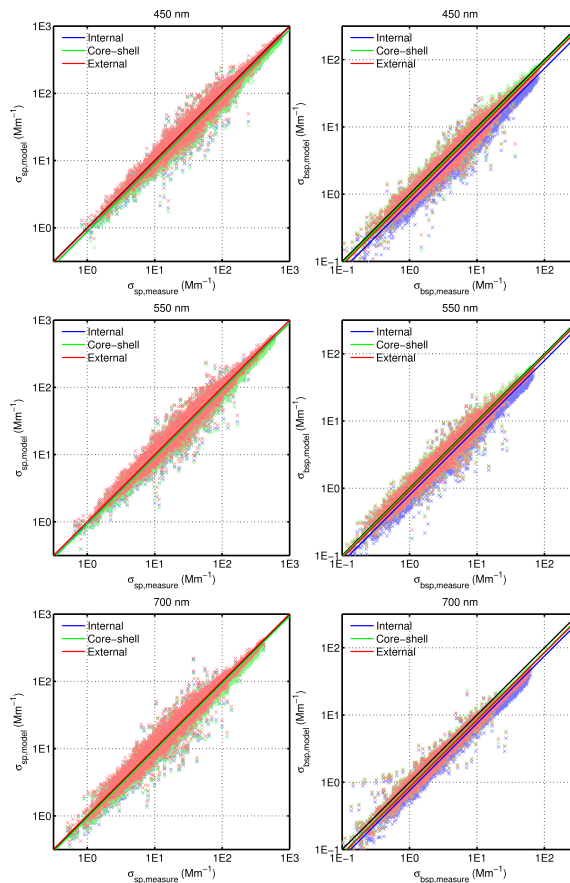


**Fig. 1.** Comparisons of measured and calculated  $\sigma_{sp}$  and  $\sigma_{bsp}$  in log-scale coordinates, including the 1 : 1 reference lines. The straight lines represent the linear regression fits to the log-scaled data. Colors denote different assumptions of aerosol mixing state for the calculations.



## Tropospheric aerosol scattering and absorption over Central Europe

N. Ma et al.

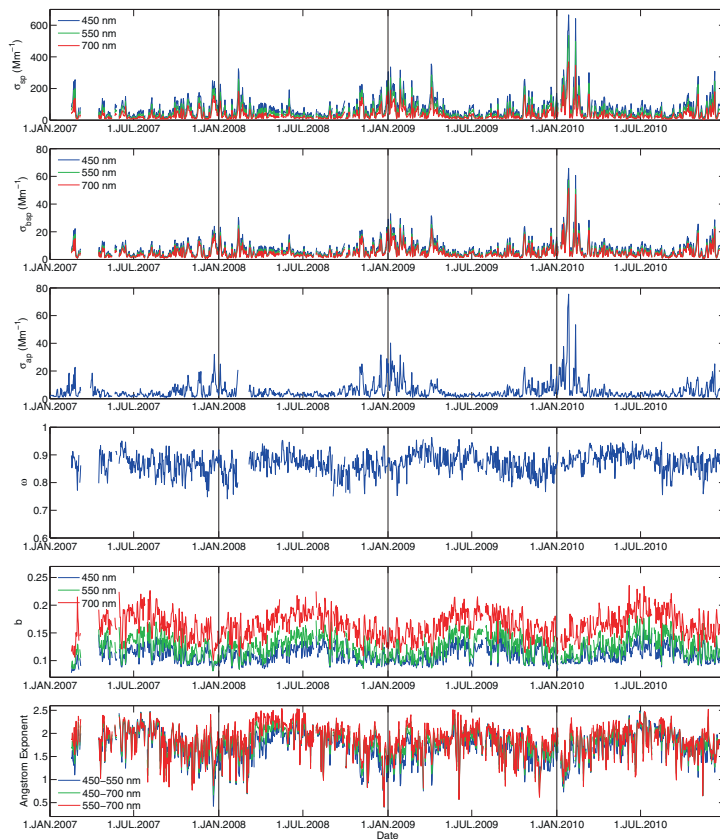


**Fig. 3.** Time series of daily average aerosol optical parameters for the extended measurement period 2007–2010. The six panels illustrate the scattering coefficient, hemispheric backscattering coefficient, absorption coefficient, single scattering albedo, hemispheric backscattering fraction and Ångström exponent.

## Tropospheric aerosol scattering and absorption over Central Europe

N. Ma et al.

Title Page

Abstract

Introduction

Conclusions

References

Tables

Figures

◀

▶

◀

▶

Back

Close

Full Screen / Esc

Printer-friendly Version

Interactive Discussion

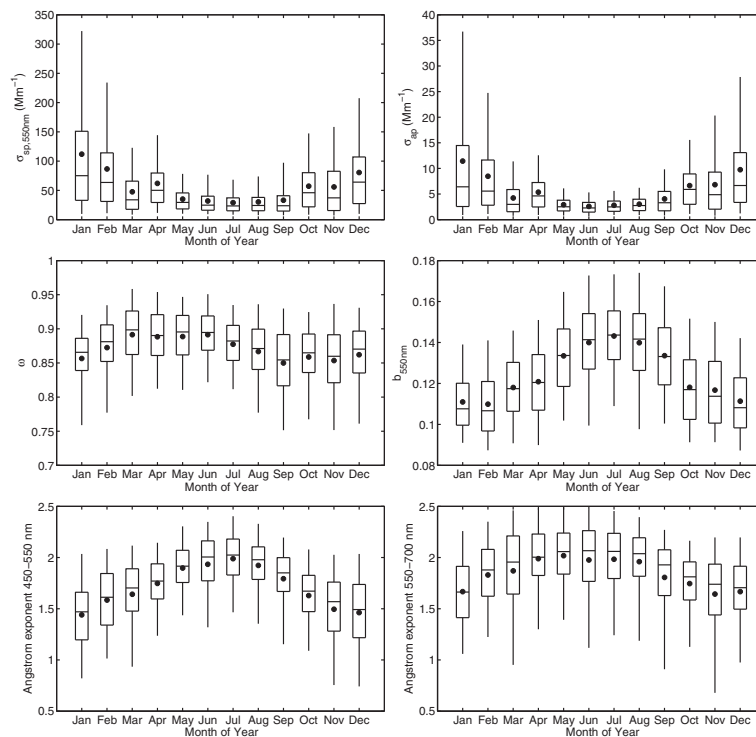


**Fig. 4.** Annual variations of aerosol scattering coefficient (top left), absorption coefficient (top right), single scattering albedo (middle left), hemispheric backscattering fraction (middle right), Ångström exponent at 450–550 nm (bottom left) and at 550–700 nm (bottom right). For each panel, the boxes and whiskers denote the 5, 25, 50, 75 and 95 percentiles, while the dots denote the mean values.

## Tropospheric aerosol scattering and absorption over Central Europe

N. Ma et al.

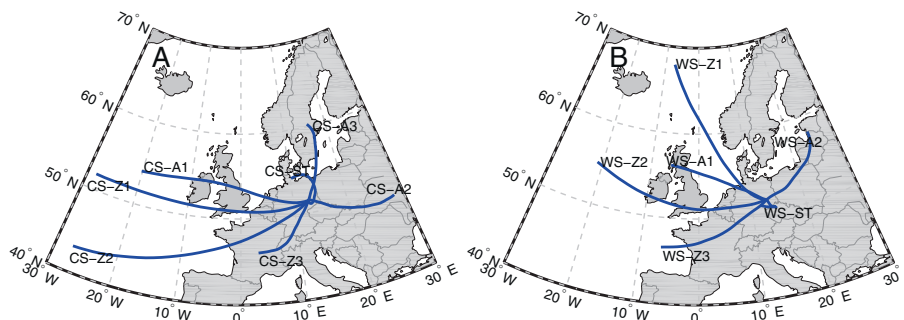


**Fig. 5.** Average back trajectories (72 h) for 13 air mass types. **(A)** and **(B)** are respectively for cold season and warm season.

[Title Page](#)[Abstract](#)[Introduction](#)[Conclusions](#)[References](#)[Tables](#)[Figures](#)[⏪](#)[⏩](#)[◀](#)[▶](#)[Back](#)[Close](#)[Full Screen / Esc](#)[Printer-friendly Version](#)[Interactive Discussion](#)

## Tropospheric aerosol scattering and absorption over Central Europe

N. Ma et al.

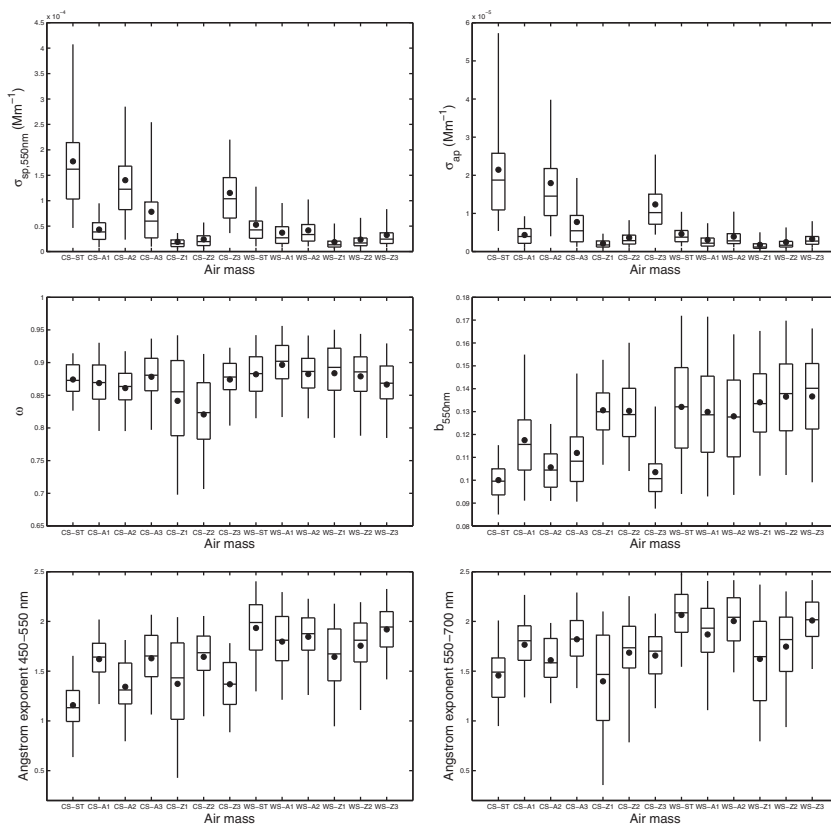


**Fig. 6.** Average aerosol scattering coefficient (top left), absorption coefficient (top right), single scattering albedo (middle left), hemispheric backscattering fraction (middle right), Ångström exponent at 450–550 nm (bottom left) and at 550–700 nm (bottom right) for the 13 air mass types. For each panel, the boxes and whiskers denote the 5, 25, 50, 75 and 95 percentiles, while the dots denote the mean values.

Title Page	
Abstract	Introduction
Conclusions	References
Tables	Figures
◀	▶
◀	▶
Back	Close
Full Screen / Esc	
Printer-friendly Version	
Interactive Discussion	

## Tropospheric aerosol scattering and absorption over Central Europe

N. Ma et al.

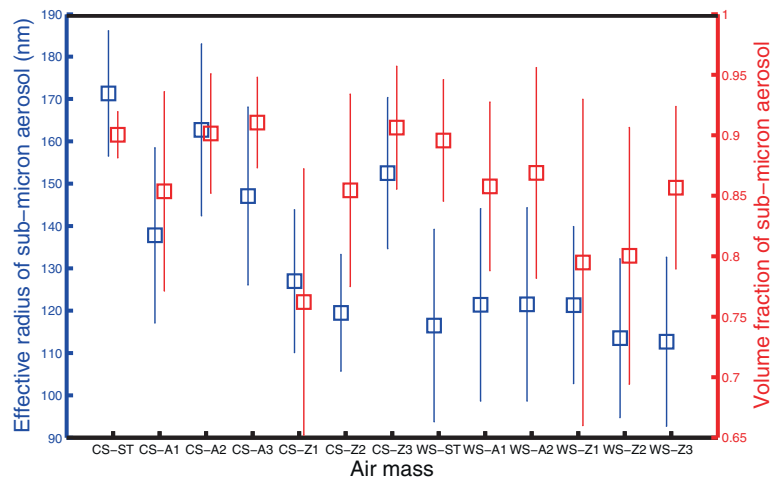


**Fig. 7.** Average effective radius (blue) and volume fraction of sub-micron aerosol for the 13 air mass types. Whiskers denote the standard deviation.

Title Page

Abstract

Introduction

Conclusions

References

Tables

Figures

◀

▶

◀

▶

Back

Close

Full Screen / Esc

Printer-friendly Version

Interactive Discussion